PAPER

Check for updates

Impedimetric detection of 2,4,6-trinitrotoluene using surface-functionalized halloysite nanotubes†

Supak Pattaweepaiboon, [ID] [a] Varuntorn Pimpakoon,[a] Nattida Phongzitthiganna, [ID] [ab] Weekit Sirisaksoontorn, [ID] [ab] Kannika Jeamjumnunja [ID] *[ab] and Chaiya Prasittichai [ID] *[ab]

Herein, we report the application of amine-surface-functionalized halloysite nanotubes (HAs) as active materials for the quantitative detection of 2,4,6-trinitrotoluene (TNT). The findings indicated that HA could selectively capture TNT *via* a strong reaction between the amine groups on its surface and the TNT molecules. Plate electrodes were fabricated from HA to evaluate its TNT-sensing capacity by electrochemical impedance spectroscopy. Upon binding with TNT, the proton conductivity on the HA plate electrodes increased linearly with the TNT concentration from 1.0×10^{-11} M to 1.0×10^{-4} M. The HA plate electrodes exhibited good sensitivity with a detection limit of 1.05×10^{-12} M. Subsequently, the cycling measurements of the TNT binding/removal were performed on the HA plate electrode, and the material exhibited high stability, good regenerative ability, and good reversibility without a significant decrease in efficiency. The present work highlights the significant application potential of HAs for the electrochemical detection of TNT.

Introduction

The compound 2,4,6-trinitrotoluene (TNT) is a generally known nitroaromatic explosive material. It is extensively employed in military activities, mining, and various industrial processes, including textile dye/agrochemical production and chemical syntheses.[1–4] However, TNT is highly toxic, carcinogenic, and biologically persistent. Reports have indicated that direct exposure to a certain level of TNT can induce skin irritation, anemia, and abnormal liver function.[2,5,6] The contamination of soil and groundwater with TNT, resulting from its improper handling, processing, and disposal, is a major source of hazardous environmental pollution.[7,8] Consequently, rapid and reliable methods for the trace detection of TNT are of great importance for public security and environmental monitoring.

A variety of methods have been reported for the detection and analysis of TNT and other explosives in environmental samples, including mass spectrometry, ion-mobility spectroscopy, fluorescence spectroscopy, surface-enhanced Raman scattering, and gas and liquid chromatography.[9–16] However, these methods require intricate equipment and involve complicated procedures.[6,17] In addition, it is difficult to miniaturize and implement these systems into hand-held devices for real-time applications. Recently, the electrochemical method has emerged as an attractive detection system for the on-site measurement of nitroaromatic explosives owing to its high specificity and sensitivity, manipulation simplicity, portability, and low cost.[18,19] Extensive efforts have been devoted to the development of suitable chemical platforms for the electrochemical detection of TNT.[2,20–26] For instance, Ho *et al.*[27] reported an interesting application of electrochemical impedance spectroscopy (EIS) to detect TNT in the sandwich structure of amine-functionalized gold film electrodes, TNT, and an anti-TNT aptamer. A good detection limit and a dynamic range of 10^{-14} M TNT and 10^{-14}–10^{-3} M, respectively, were achieved. Furthermore, Zhang *et al.*[28] implemented a smartphone-based impedance-monitoring system using screen-printed electrodes modified with TNT-specific peptides as biosensors. This system could detect compounds at concentrations of as low as 10^{-6} M. These results validate the potential of EIS for TNT detection and highlight a path for portable TNT-sensing systems. However, these chemical platforms use molecular recognition biomaterials, such as aptamers, antibodies, and peptides, which require a complicated selection of biomolecules with high affinity and selectivity toward their specific targets. In addition, these materials must be stored under controlled conditions to maintain their stability and activity.[23,28,29]
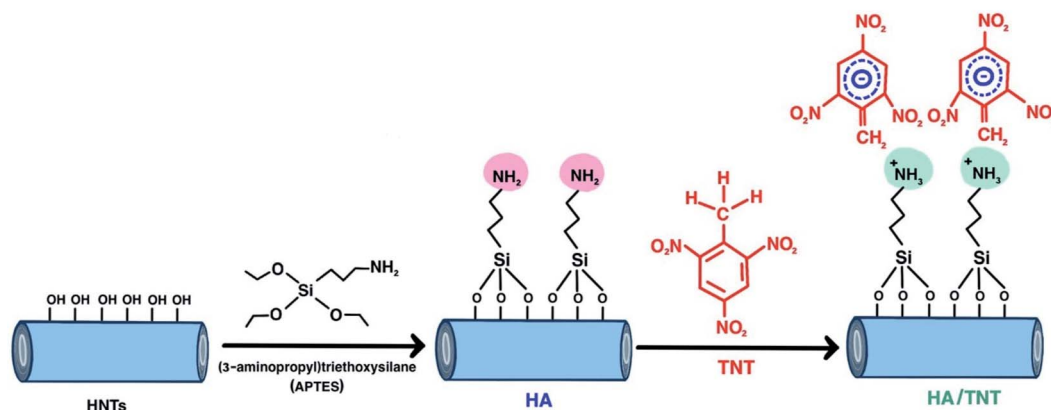
Considering that amine groups can selectively react with TNT molecules,[30–32] amine-based materials have been extensively developed for the detection and determination of TNT. The interaction between TNT and primary amines occurs *via* two mechanisms.[30] First, the electron-rich amine transfers

[a]*Department of Chemistry, Faculty of Science, Kasetsart University, Bangkok 10900, Thailand. E-mail: fscicyp@ku.ac.th; chaiya.pr@ku.th*

[b]*Center of Excellence for Innovation in Chemistry, Faculty of Science, Kasetsart University, Bangkok 10900, Thailand*

† Electronic supplementary information (ESI) available. See https://doi.org/10.1039/d2ra02482a

Scheme 1 Schematic of surface modification of HNTs with APTES to produce amine-functionalized HNTs (HA), followed by the interaction of NH_2 functional groups on the surface of HA with TNT.

a charge to the electron-deficient aromatic ring of TNT, which leads to the formation of a Meisenheimer complex.[31] Second, the TNT acts as a Brønsted–Lowry acid, forming an acid–base pairing with the basic amine. Subsequently, the methyl group of TNT is deprotonated by the primary amine, and the negative charge on the TNT anion is distributed throughout the molecule *via* resonance stabilization by three electron-withdrawing nitro groups.[33] Both the TNT anion and TNT–amine complex can strongly absorb green light and exhibit a deep red color.[31,34] Reports have demonstrated that TNT can be detected and captured using (3-aminopropyl)triethoxysilane (APTES)-surface-functionalized materials. Numerous probing methods based on APTES-functionalized materials have been reported, including colorimetry, fluorescence quenching, or molecular imprinting techniques on silica nanomaterials,[8,31,33,35] surface plasmon resonance using gold-coated sensor chips,[36] and sensing techniques using field-effect transistors with silicon nanowires.[30]

Halloysite nanotubes (HNTs) are naturally occurring aluminosilicate minerals with unique properties, including high natural abundance, low cost, and high chemical and mechanical stability.[37–39] HNTs have a hollow tubular structure, diameters typically smaller than 100 nm, and lengths of several hundred nanometers.[40,41] The inner and outer surfaces of HNTs consist of the aluminol (Al–OH) and siloxane (Si–O–Si) groups, respectively, which are chemically reactive and can, thus, be modified to enhance their surface properties for various applications, including electrochemical sensing, drug-delivery support, and catalysis.[42–45] Recently, we reported an electrochemical CO_2 sensor based on amine-modified HNTs using EIS as a detection method.[46]

In this study, the surface functionalization of HNTs with APTES was performed using a self-assembled monolayer (SAM) method to produce amine-functionalized HNTs (HA) (Scheme 1). The application of HA for the electrochemical sensing of TNT was investigated *via* EIS. Plate electrodes were fabricated from the HA materials for use in the conductivity analysis using the AC impedance method (2-point probe). The changes in the proton conductivity of HA upon binding with TNT at different concentrations were measured. In addition, the sensing properties of HA, including its selectivity, stability, reusability, and regenerative ability, were examined.

Experimental section

Materials and chemicals

The HNTs and APTES ($C_9H_{23}NO_3Si$, 99% purity) were purchased from Sigma-Aldrich. TNT and 2,4-dinitrotoluene (DNT) were generously provided by the Army Research and Development Office of Thailand. The compounds 2,4-dinitrophenol (2,4-DNP) and 4-nitrophenol (4-NP) were purchased from Tokyo Chemical Industry Co., Ltd. Toluene, ethanol, and acetonitrile were purchased from Emsure, Carlo Erba Reagents, and Burdick & Jackson, respectively. All reagents were of analytical grade and used as received without further purification.

Synthesis of HA

To synthesize HA, we followed the procedures presented in our recently published work.[46] Briefly, 1 g of the HNTs in a round-bottom flask was purged with N_2 gas for 25 min. Thereafter, approximately 12 mL of toluene was injected into the flask. The mixture solution in a N_2 atmosphere was continuously stirred and heated to 60 °C. Subsequently, the APTES solution was injected into the round-bottom flask. Shortly after, the temperature of the resulting mixture solution under a N_2 atmosphere was increased to 120 °C and maintained for 8 h. Next, the suspension was centrifuged. The white HA powder was separated and washed three times with toluene and ethanol, separately, after which it was oven-dried at 120 °C for 18 h.

Preparation of the HA/TNT powder samples

The solution of TNT was prepared in different concentrations ranging from 1.0×10^{-11} M to 1.0×10^{-4} M in the ethanol/acetonitrile (80 : 20 v/v) solvent system. The colorless solution of TNT (0.5 mL) was poured into the vial containing the white powder of HA (0.25 g), which equals a liquid-to-solid ratio of 2 : 1. After mixing the HA powder and TNT solution, a red Meisenheimer complex was observed. Subsequently, the

suspension of HA/TNT was allowed to stand overnight at room temperature to ensure the complete evaporation of the solvent. Finally, the dried powder of the HA/TNT samples was collected for characterization and EIS measurements.

Characterization

The thermal stability of the HNTs and HA samples was investigated *via* thermogravimetric analysis (TGA, PerkinElmer, TGA 7) in the temperature range of 30 °C–800 °C, at a heating rate of 10 °C min^{-1} under a N_2 atmosphere.

Attenuated total reflectance-Fourier transform infrared (ATR-FTIR) spectroscopy was conducted on a Bruker Vertex70 FTIR spectrometer in the region of 4000–400 cm^{-1}. The surface morphologies of the HA and HA/TNT samples were investigated by scanning electron microscopy (SEM) using an FEI Quanta 540 microscope. The sample surface was sputtered with conductive gold before the SEM measurements being performed. The X-ray photoelectron spectra were recorded using a PHI 5000 Versa Probe II XPS system (ULVAC-PHI, Japan) with Al Kα (1486.6 eV) as an X-ray source. The obtained X-ray photoelectron spectroscopy (XPS) data were analyzed using CasaXPS software. The UV-vis absorption spectra were recorded on a PerkinElmer Lambda 365 UV-Vis spectrophotometer.

EIS measurements

The changes in the proton conductivity of the unmodified and modified HNTs upon binding with TNT were measured *via* EIS. A plate electrode with a 2 mm thickness was constructed by pressing the powder sample ($\sim$0.25 g) of HA/TNT or HNTs/TNT of various TNT concentrations between two sheets of nickel foam in a pellet die (diameter: 10 mm) under a hydraulic pressure of 0.3 metric tons. Both sides of the plate electrode were coated with conductive silver epoxy (types A and B, Chemtronics) and connected to copper wires. Subsequently, the plate electrode was heated to 60 °C for 30 min in an oven to dry the conductive epoxy. Before the EIS measurements, methanol vapor was introduced to the plate electrode for 60 s, after which the plate electrode was electrically connected to an impedance spectrometer (PalmSens, PalmSens4 potentiostat). EIS measurements were performed at room temperature (35 °C $\pm$ 2 °C) with an AC perturbation of 20 mV and over a frequency range of 1–10^6 Hz, without applying DC voltage. Subsequently, the impedance data were quantitatively interpreted by fitting them to an equivalent circuit model (Randles circuit). The analysis was conducted using the PSTrace software version 5.7. All the EIS evaluations were conducted on, at least, three plate electrodes at the same concentration to ensure the consistency of the measurements.

The selectivity measurement toward TNT was performed with other nitroaromatics, including 2,6-dinitrotoluene (2,6-DNT), 2,4-dinitrophenol (2,4-DNP), and 4-nitrophenol (4-NP). Experiments were conducted by mixing 0.50 mL of each of these interference materials at a concentration of 10^{-6} M with 0.25 g of the HA powder and subsequently measuring the change in the proton conductivity. The procedures for sample preparation

and EIS analysis were done in a similar fashion, as previously described for TNT.

The procedure used to regenerate the HA/TNT in this work was obtained by modifying a previously reported method.[47,48] The TNT-binding/removal cycling experiments were conducted by EIS to evaluate the stability and reversibility of the HA plate electrode. The changes in the impedance of the HA/TNT plate electrode were measured with respect to the TNT-binding cycle. Thereafter, the regeneration step was performed by adding 5 mL of ethanol into the powder sample of HA/TNT to remove the TNT molecules that were bound to the HA surface. Next, the suspension was stirred at room temperature for approximately 10 min and centrifuged to collect the solid samples of HA. All the regeneration steps were repeated three times to ensure that the free HA was obtained. After the regeneration, the impedance changes were measured on the plate electrode of the obtained samples with respect to the TNT-removal cycle. The resistance value of the plate electrode of the pure HA was considered as the baseline for the TNT-removal cycle.

Results and discussion

Characterization of the HNTs and HAs

The internal and external surfaces of the HNT nanotubes mainly consist of aluminol (Al–OH) and siloxane (Si–O–Si), respectively, which allow different inner/outer surface chemistries and selective surface functionalization.[49,50] The silanol (Si–OH) groups occurring at the crystal defects of the external surface provide the accessibility for the surface functionalization.[45,50,51] In this work, the selective surface functionalization of HNTs with APTES was performed using the SAM method to obtain amine-functionalized HNTs, according to the procedures reported in our previous work.[46] The SAM pattern of APTES was grafted onto the HNT surface through the Si–O–Si bonding occurring between the surface Si–OH groups of the HNTs and the polysiloxane groups of APTES (Scheme 1).[52] In our previous work,[46] the effect of APTES concentration used in the synthesis of HA was investigated using APTES concentration ranging from 2 wt% to 70 wt%. The grafting density of APTES indicated that the surfaces of the HNTs were saturated upon the addition of 20 wt% APTES, which was found to be an optimal concentration, and thus selected for use in the present work.

The FTIR spectra of the HNTs and HAs (see Fig. 1) were recorded to examine the chemical changes after the grafting of APTES on the HNT surface. The peak positions and corresponding assignments of both samples are given in Table S1 in ESI.† The assignments are consistent with those in our previous work[46] and other reports on APTES-functionalized HNTs.[53,54] In the spectra of both the HNTs and HA, the well-defined peaks at 3695 and 3622 cm^{-1} are assigned to the stretching vibration of the outer- and inner-surface hydroxyl groups, respectively. The bands at around 1120 and 1030 cm^{-1} can be attributed to the perpendicular and in-plane Si–O stretching. In the enlarged FTIR spectrum (see the inset in Fig. 1), new peaks for HA can be observed at 3456 and 2932 cm^{-1}, corresponding to the N–H stretching and C–H$_2$ stretching, respectively, and at 1568 and 1487 cm^{-1}, corresponding to the deformation of N–H$_2$ and C–
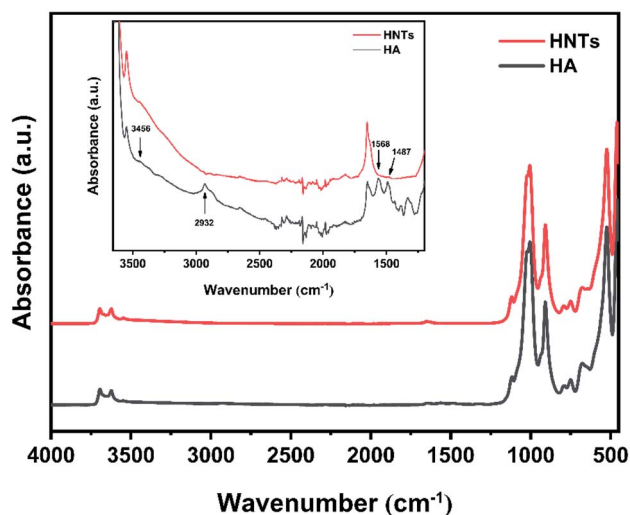
Fig. 1 FTIR spectra of the HNTs and HA. The inset shows the chemical changes due to the grafting of APTES on the surface of HNTs in the region of 3655–1200 cm^{-1}.

H_2, respectively. The FTIR results validated the successful surface functionalization of the HNTs with APTES.

The thermal decomposition behaviors of both the HNTs and HA were examined *via* TGA in the temperature range of 30 °C–800 °C under a N_2 atmosphere to determine the amount of APTES grafted onto the HNT surface. The TGA and derivative thermogravimetric (DTG) curves of the raw HNTs and HA are presented in Fig. S1, ESI.† Both materials exhibited two weight-loss steps at 30 °C–150 °C, corresponding to the desorption of physisorbed water from the surface of the HNTs, and above 350 °C, associated with the dehydroxylation of the Al–OH and Si–OH groups of the HNTs.[51,54–56] For the HA sample, the additional decomposition of the APTES species grafted onto the Al–OH and Si–OH groups on the HNT surface was observed in the temperature range of 250 °C–350 °C.[54] The weight losses of both the HNTs and HA obtained from the TGA data are presented in Table S2, ESI.† The amount of APTES grafted onto the surface of HNTs was calculated from the weight loss of HA at 250–800 °C using the equation presented in our previous work.[46] The grafting density was equal to 6.74 APTES molecules per square nanometer of the HNTs, which was consistent with the value obtained in the previous work.[46]

Interaction of the HAs and TNT

The interaction between the TNT and HAs was investigated by adding the white powder of HA into the colorless solution of TNT in a liquid-to-solid ratio of 2 : 1 (mL of TNT solution per gram of dry material). The TNT solution was prepared in various concentrations ranging from 1.0×10^{-4} M to 1.0×10^{-11} M in the ethanol/acetonitrile (80 : 20, v/v) solvent system. After mixing the HA powder and TNT solution, a red Meisenheimer complex was apparently formed by the reaction between the TNT molecules and the amine head groups attached to the HA surface. A gradual change in color to dark red was observed

when the TNT concentration was increased, as presented in Fig. S2, ESI.† The suspension of HA/TNT was subsequently stored overnight at room temperature until the solvent was completely evaporated. The dried powder of the HA/TNT samples was collected for the FTIR and EIS measurements. Notably, the red color of the HA/TNT powder samples appeared lighter than that of the suspension (Fig. S2†). This could be due to the increased chemical stability of the Meisenheimer complex, which can be attributed to the solvation effect. The apparent colorimetric detection limit for the naked eye was 10^{-6} M of TNT. In addition, UV-vis spectroscopy was performed on the powder samples of HNTs, HA, and HA/TNT with the addition of 10^{-4} M TNT in the region of 400–750 nm, the results of which are presented in Fig. S3, ESI.† While there is no absorption peaks observed in the spectra of HNTs and HA (Fig. S3,† blue and black lines, respectively), as expected, the HA/TNT powder sample exhibits a broaden absorption peak centering at 520 nm (Fig. S3,† red line), which ascribes to the formation of Meisenheimer complex between amine groups on the surface of HA and TNT.

FTIR spectroscopy was employed to confirm the complex formation between HA and TNT, and the results are presented in Fig. S4, ESI.† The results indicate two distinct peaks at 1333 and 1491 cm^{-1}, assigned to the symmetric and asymmetric N═O stretching of aromatic nitro compounds, respectively.[57] The intensity of the 1333 and 1491 cm^{-1} peaks rapidly increased with the concentration of TNT, as presented in the inset of Fig. S4.†

XPS was also used to confirm the presence of complex between TNT and HA and the results are shown in Fig. S5.† The fine scan on N atom in HA shows the peaks at BE of 399 and 401 eV, corresponding to $C-NH_2$ and $C-NH_3^+$, respectively.[58] We believe that the presence of $C-NH_3^+$ in HA is mainly from water adsorption from *ex situ* analysis. Additional peak at BE of 405.9 eV, corresponding to $-NO_2$ was observed on HA/TNT, confirming the attachment of TNT on HA surface.

The surface morphologies of the HNTs, HA, and HA/TNT were examined using SEM, the results of which are displayed in Fig. S6, ESI.† SEM images of both the HNTs and HA (Fig. S6(a) and (b),† respectively) demonstrate that they have a nanotubular structure with an open-ended lumen, only the nanotubes of the HA materials become less compacted. The results show that the surface modification of HNTs with APTES does not destroy the pristine structure of HNTs. Additionally, SEM image of the HA/TNT powder at TNT concentration of 10^{-4} M (Fig. S6 (c)†) reveals that the HA/TNT consists of cylindrical-shaped nanotubes similar to those observed in the HA, indicating that the interaction between HA and TNT to produce the Meisenheimer complex of HA/TNT does not have an influence on the morphology of the HA.

EIS

HNTs and HA contain hydroxyl and amine groups in their frameworks, which can release protons into the pores, conferring proton conductivity.[46,51,59] In this work, EIS was used to study the changes in the proton conductivity arising from the

binding between the HA and TNT molecules. The powder samples obtained from the interaction between HA and TNT at different concentrations were collected and fabricated into plate electrodes for use in the AC impedance experiments. As a control experiment, the changes in the impedance of the unmodified HNTs were also investigated. Prior to any impedance measurements, all the plate electrodes were dried and subsequently saturated with methanol vapor, as previously described in the Experimental section. All impedance measurements were performed at room temperature ($\sim$35 °C $\pm$ 2 °C).

First, the AC impedance measurements were performed to measure the changes in the impedance of the plate electrodes of the pure HNTs and HNTs/TNT with added TNT at concentrations ranging from 1.0×10^{-11} M to 1.0×10^{-4} M. The obtained impedance results of all samples are shown in the Nyquist plots (Fig. S7, ESI†), in which the imaginary impedance (Z'') is plotted against the real impedance (Z'). The impedance data were quantitatively interpreted by fitting to a Randles circuit. The resistance (R) on the real impedance axis in the low-frequency range is associated with the proton transfer occurring on the plate electrode's material. The results indicate that the average resistance of the HNT plate electrodes is approximately 5.7×10^3 Ω. Meanwhile, the R values of the HNT/TNT plate electrodes were determined to range from $\sim 2.0 \times 10^3$ Ω to 3.0×10^3 Ω over the concentration range of TNT from 1.0×10^{-4} M to 1.0×10^{-11} M. The insignificant change in the proton conductivity on the HNT/TNT indicates that the unmodified HNTs are insensitive to TNT.

Next, the plate electrodes of the bare HA and HA/TNT with added TNT in concentrations ranging from 1.0×10^{-11} M to 1.0×10^{-4} M were subjected to impedance measurements. The Nyquist plots of both the bare HA and HA/TNT are presented in Fig. 2. The average R value of the bare HA taken from the impedance results is $\sim 6.5 \times 10^7$ Ω. After the interaction between HA and TNT, the plate electrodes of HA/TNT exhibited a decrease in the R values to $\sim 9.9 \times 10^6$ Ω at 1.0×10^{-11} M of TNT, and the resistance was significantly reduced to $\sim 3.2 \times 10^6$ Ω at very high concentrations of TNT over 1.0×10^{-5} M. The significant increase in the proton conductivity can be mostly attributed to the acid–base pairing mechanism between the TNT molecules and the amine groups attached to the HA surface. The methyl groups of TNT are deprotonated by a basic amine (Scheme 1), which enhances the proton-hopping mechanism and, consequently, the proton conductivity of the material. To evaluate the efficacy of HA for TNT sensing, the relationship between the impedance responses of both the HNTs and HA samples and concentrations of TNT in the range of 10^{-11}–10^{-4} M was investigated, as presented in Fig. 3. The relative change in the resistance of HA upon binding with TNT is linearly proportional to the TNT concentration, whereas the HNTs exhibited almost similar relative resistance values over the TNT concentration range. The results validate the high sensitivity of HA toward TNT. The detection limit of the HA plate electrode was calculated to be 1.05×10^{-12} M using the 3σ/slope formula.
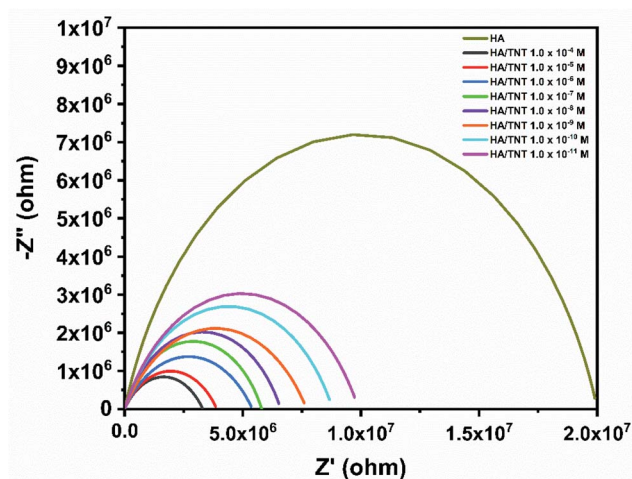

Fig. 2 Nyquist plots of the HA/TNT plate electrodes with TNT in concentrations ranging from 1.0×10^{-11} M to 1.0×10^{-4} M. Z'' and Z' are the imaginary and real impedances, respectively. The impedance data were fitted to a Randles circuit model, and only the fitted data are shown as solid lines.
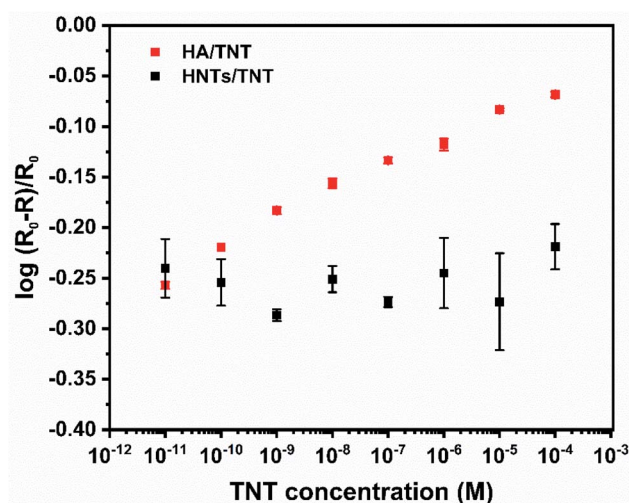

Fig. 3 Plot of the average relative resistances of the HNTs (■) and HA (■) plate electrodes as a function of the TNT concentration, where R_0 and R denote the resistances of the plate electrodes measured without and with TNT, respectively. All experiments were conducted in three replications using the same batch of samples.

To test the cross-reactivity of this detection system, impedance measurements were performed on the plate electrodes of the powder samples that were obtained from the addition of the HA into a solution of various structurally-related nitroaromatics at a concentration of 1.0×10^{-6} M, including TNT, 2,6-dinitrotoluene (2,6-DNT), 2,4-dinitrophenol (2,4-DNP), and 4-nitrophenol (4-NP), whose chemical structures are presented in Fig. S8, ESI.† The resistance values of the HA plate electrodes measured with these nitroaromatics are summarized in Table S3, ESI.† The changes in the resistance of the HA/TNT plate electrode are significantly stronger than those of other nitro-
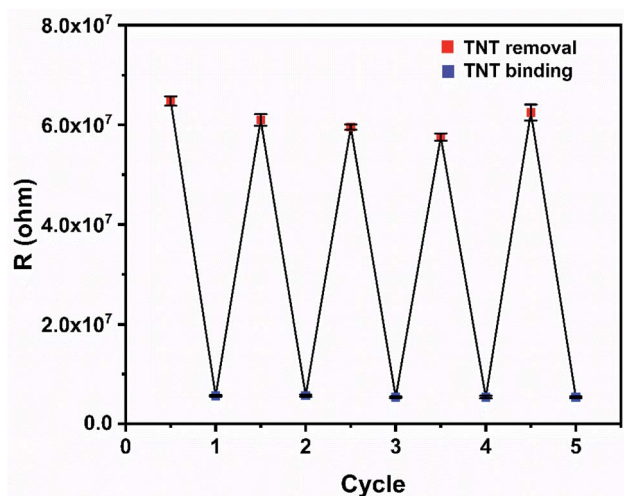
Fig. 4 Changes in the resistance of the HA plate electrodes during the TNT-binding (■)/removal (■) cycling experiments. The TNT-binding cycles were conducted with a TNT concentration of 1.0×10^{-6} M. Three replications of all the experiments were performed using the same batch of samples.

substituted aromatics (Fig. S8, ESI†). It was also noted that the resistance changes of the plate electrode of HA and the added 2,4-DNP or 4-NP are approximately half those of TNT. This is likely attributed to the formation of the phenolate complex by the acid–base pairing reaction between the phenolic groups of these two molecules and the amine groups on the HA surface,[32] which results in an increase in the proton mobility of the material and, consequently, a reduction in the resistance, similar to the event that occurred between HA and TNT. However, the results clearly indicate that the TNT molecules with a high electron-withdrawing nature have a higher ability to react with the amine groups attached to the surface of HA than the others, thus confirming that HA is more selective toward TNT.

Finally, an important issue to consider for the application of this material in a real-time field sensor is its ability to rapidly regenerate after operation. Therefore, TNT-binding/removal cycling experiments were conducted using EIS to demonstrate the reversibility and stability of the HA plate electrodes. The changes in the impedance of the HA/TNT plate electrode were measured with respect to the TNT-binding cycle. After the reaction of TNT and HA, ethanol, as the washing solution, was introduced into the HA/TNT mixture to remove the TNT from the system according to the procedures discussed in the Experimental section; thereafter, the impedance changes were measured on the plate electrode of the obtained samples with respect to the TNT-removal cycle. The resistance value obtained from the plate electrode of the pure HA was considered as the baseline value for the system without TNT. The resistance values obtained from fitting the impedance data to the Randles circuit are summarized in Table S4, ESI† and presented in Fig. 4. The HA plate electrode exhibited a high degree of reversibility during the TNT-binding/removal cycles. The R value of the plate electrode decreased from $\sim 6.0 \times 10^7$ Ω to $\sim 5.4 \times 10^6$ Ω after binding with TNT at a concentration of 1.0×10^{-6} M (*i.e.*, an increase in the proton conductivity by a factor of ~ 10 fold), and the resistance reverted to the baseline value after the removal of TNT. This process is completely reversible, without a significant decrease in performance, evidencing the significant sensing stability and reproducibility of the HA plate electrode for the TNT detection.

Table 1 shows some examples of the materials reported recently as a chemical platform for electrochemical detection of TNT and their detection limit. Of these, the electrochemical aptamer-based assay exploiting the interaction of TNT and primary amine and TNT with the aptamer has the lowest detection limit of 10^{-14} M TNT,[27] however, the aptamer is an recognition biomaterial which requires a complicated selection with high affinity and selectivity toward specific targets and must be stored under controlled conditions to maintain their stability and activity.[23,28,29] The APTES-functionalized halloysite nanotubes (HA) using EIS as a detection method proposed in the present work has the second lowest detection limit with high sensing stability and reversibility. Though, it may require somewhat long time to synthesize HA in the laboratory (16 hours), the process is, however, straightforward, doesn't require special treatment and could be stored at room temperature. As a result, we believe that this material could be potentially employed to test TNT in field study. In fact, we are currently working on utilizing this material in screen-printed electrode and will present the results in the future.

Table 1 Detection limit of TNT and detection technique of some materials using as a chemical platform for electrochemical detection of TNT

Material	Detection limit of TNT (M)	Detection technique	Ref.
TiO$_2$ nanotube arrays	4.4×10^{-4}	Cyclic voltammograms	22
Polyaniline/gold nanoparticles/carbon nanotubes composite electrodes	4.84×10^{-12}	Cyclic voltammograms	60
Gold nanoparticles/poly(carbazole-aniline) film-modified glassy carbon electrode	1.10×10^{-7}	Cyclic voltammograms	61
Poly(styrene-*co*-acrylic acid) PSA/SiO$_2$/Fe$_3$O$_4$/AuNPs/lignin-modified glassy carbon electrode	3.5×10^{-11}	Cyclic voltammograms	62
Single-, few-, and multilayer graphene nanoribbons and graphite microparticles	4.40×10^{-6}	Cyclic voltammograms	63
Carbon nanotube modified electrode	1×10^{-6}	Cyclic voltammograms	64
Ionic liquid gel-polymer electrolyte film	1.63×10^{-6}	Cyclic voltammograms	65
Aptamer-based assay with amine functionalized gold film electrodes	1×10^{-14}	EIS	27
Screen-printed electrodes modified with TNT-specific peptides	1×10^{-6}	EIS	28
(3-Aminopropyl)triethoxysilane (APTES)-functionalized halloysite nanotubes	1.05×10^{-12}	EIS	This work

Conclusions

The surface functionalization of HNTs with APTES to produce the amine-functionalized HNTs was achieved using the SAM technique. The HA plate electrodes were fabricated and used as an electrochemical sensor for the detection and quantification of TNT with EIS as the detection method. The proton conductivity of the HA/TNT plate electrodes increased. This was attributed to an increase in the proton mobility during the acid–base pairing reaction between the TNT molecules and the amine groups attached to the HA surface. The correlation between the proton conductivity on the HA plate electrode and the change in the TNT concentration from 1.0×10^{-11} M to 1.0×10^{-4} M revealed that the proton conductivity linearly increases with the TNT concentration. The HA plate electrode was selective toward TNT with good sensitivity. The detection limit of the system obtained from the calculation using the 3σ/slope equation was 1.05×10^{-12} M. In addition, the HAs were highly stable and exhibited excellent reversibility during the TNT-binding/removal cycles without any significant reduction in efficiency. Therefore, this study highlights the significant application potential of HA for the electrochemical sensing of TNT.

Author contributions

The manuscript was written through contributions of all authors. All authors have given approval to the final version of the manuscript prior to submission.

Funding sources

Conflicts of interest

There are no conflicts to declare.

Abbreviations

HA	Amine-surface-functionalized halloysite nanotube
TNT	2,4,6-Trinitrotoluene
EIS	Electrochemical impedance spectroscopy
APTES	(3-Aminopropyl)triethoxysilane
HNT	Halloysite nanotube
SAM	Self-assembled monolayer
TGA	Thermogravimetric analysis
FTIR	Fourier-transform infrared
R	Resistance

Acknowledgements

References

1 A. Fainberg, Explosives Detection for Aviation Security, *Science*, 1992, **255**, 1531–1537.

2 D. Niea, D. Jianga, D. Zhanga, Y. Lianga, Y. Xuea, T. Zhoub, L. Jin and G. Shia, Two-Dimensional Molecular Imprinting Approach for the Electrochemical Detection of Trinitrotoluene, *Sens. Actuators, B*, 2011, **156**, 43–49.

3 Ç. Özcan, A. Üzer, S. Durmazel and R. Apak, Colorimetric Sensing of Nitroaromatic Energetic Materials Using Surfactant-Stabilized and Dithiocarbamate-Functionalized Gold Nanoparticles, 2019 Nanoparticles, *Anal. Lett.*, 2019, **52**(17), 2794–2808.

4 H. Sohn, M. J. Sailor, D. Magde and W. C. Trogler, Detection of Nitroaromatic Explosives Based on Photoluminescent Polymers Containing Metalloles, *J. Am. Chem. Soc.*, 2003, **125**, 3821–3830.

5 S. S. R. Dasary, A. K. Singh, D. Senapati, H. Yu and P. C. Ray, Gold Nanoparticle Based Label-Free SERS Probe for Ultrasensitive and Selective Detection of Trinitrotoluene, *J. Am. Chem. Soc.*, 2009, **131**, 13806–13812.

6 N. Tang, L. Mu, H. Qu, Y. Wang, X. Duan and M. A. Reed, Smartphone-Enabled Colorimetric Trinitrotoluene Detection Using Amine-Trapped Polydimethylsiloxane Membranes, *ACS Appl. Mater. Interfaces*, 2017, **9**, 14445–14452.

7 S. S. R. Dasary, D. Senapati, A. K. Singh, Y. Anjaneyulu, H. Yu and P. C. Ray, Highly Sensitive and Selective Dynamic Light-Scattering Assay for TNT Detection Using *p*-ATP Attached Gold Nanoparticle, *ACS Appl. Mater. Interfaces*, 2010, **2**, 3455–3460.

8 N. Idros, M. Y. Ho, M. Pivnenko, M. M. Qasim, H. Xu, Z. Gu and D. Chu, Colorimetric-Based Detection of TNT Explosives Using Functionalized Silica Nanoparticles, *Sensors*, 2015, **15**, 12891–12905.

9 S. Babaeea and A. Beiraghib, Micellar Extraction and High Performance Liquid Chromatography-Ultra Violet Determination of Some Explosives in Water Samples, *Anal. Chim. Acta*, 2010, **662**, 9–13.

10 X. He, H. Wang, Z. Li, D. Chen and Q. Zhang, ZnO–Ag Hybrids for Ultrasensitive Detection of Trinitrotoluene by Surface-Enhanced Raman Spectroscopy, *Phys. Chem. Chem. Phys.*, 2014, **16**, 14706–14712.

11 T. Liu, K. Zhao, K. Liu, L. Ding, S. Yin and Y. Fang, Synthesis, Optical Properties and Explosive Sensing Performances of a Series of Novel π-Conjugated Aromatic End-Capped Oligothiophenes, *J. Hazard. Mater.*, 2013, **246–247**, 52–60.

12 D. Marder, N. Tzanani, H. Prihed and S. Gura, Trace Detection of Explosives with a Unique Large Volume Injection Gas Chromatography-Mass Spectrometry (LVI-GC-MS) Method, *Anal. Methods*, 2018, **10**, 2712–2721.

13 B. R. Smedts, W. Baeyens and H. C. D. Bisschop, Separation of Arsines and Trinitrotoluene by Reversed Phase High Performance Liquid Chromatography and Micellar Electrokinetic Capillary Chromatography, *Anal. Chim. Acta*, 2003, **495**, 239–247.

14 P. Sulzer, F. Petersson, B. Agarwal, K. H. Becker, S. Jürschik, T. D. Märk, D. Perry, P. Watts and C. A. Mayhew, Proton Transfer Reaction Mass Spectrometry and the Unambiguous Real-Time Detection of 2,4,6 Trinitrotoluene, *Anal. Chem.*, 2012, **84**, 4161–4166.

15 C. Zhang, K. Wanga, D. Han and Q. Pang, Surface Enhanced Raman Scattering (SERS) Spectra of Trinitrotoluene in Silver Colloids Prepared by Microwave Heating Method, *Spectrochim. Acta, Part A*, 2014, **122**, 387–391.

16 X. Zhao and J. Yinon, Characterization and Origin Identification of 2,4,6-Trinitrotoluene through Its by-Product Isomers by Liquid Chromatography–Atmospheric Pressure Chemical Ionization Mass Spectrometry, *J. Chromatogr. A*, 2002, **946**(1–2), 125–132.

17 S. Huang, Q. He, S. Xu and L. Wang, Polyaniline-Based Photothermal Paper Sensor for Sensitive and Selective Detection of 2,4,6-Trinitrotoluene, *Anal. Chem.*, 2015, **87**, 5451–5456.

18 J. Wang, Electrochemical Sensing of Explosives, *Electroanalysis*, 2007, **19**(4), 415–423.

19 H.-X. Zhang, J.-S. Hu, C.-J. Yan, L. Jiang and L. J. Wan, Functionalized Carbon Nanotubes as Sensitive Materials for Electrochemical Detection of Ultra-Trace 2,4,6-Trinitrotoluene, *Phys. Chem. Chem. Phys.*, 2006, **8**, 3567–3572.

20 X.-C. Fu, X. Chen, J. Wang, J.-H. Liu and X.-J. Huang, Amino Functionalized Mesoporous Silica Microspheres with Perpendicularly Aligned Mesopore Channels for Electrochemical Detection of Trace 2,4,6-Trinitrotoluene, *Electrochim. Acta*, 2010, **56**, 102–107.

21 D. N. Mazaafrianto, A. Ishida, M. Maeki, H. Tani and M. Tokeshi, Label-Free Electrochemical Sensor for Ochratoxin A Using a Microfabricated Electrode with Immobilized Aptamer, *ACS Omega*, 2018, **3**, 16823–16830.

22 S. Moon, N. L. Reddy, J. Lee, H. Lee, W. Lee and K. Lee, Electrochemical Detection of 2,4,6-Trinitrotoluene Reduction in Aqueous Solution by Using Highly Ordered 1D TiO$_2$ Nanotube Arrays, *Mater. Today Commun.*, 2020, **25**, 101389.

23 W. Qi, M. Xu, L. Pang, Z. Liu, W. Zhang, S. Majeed and G. Xu, Electrochemiluminescence Detection of TNT by Resonance Energy Transfer through the Formation of a TNT–Amine Complex, *Chem. - Eur. J.*, 2014, **20**, 4829–4835.

24 J. Wang, S. B. Hocevar and B. Ogorevc, Carbon Nanotube-Modified Glassy Carbon Electrode for Adsorptive Stripping Voltammetric Detection of Ultratrace Levels of 2,4,6-Trinitrotoluene, *Electrochem. Commun.*, 2004, **6**, 176–179.

25 Q. Yang, Y. Liang, T. Zhou, G. Shi and L. Jin, TNT Determination Based on Its Degradation by Immobilized HRP with Electrochemical Sensor, *Electrochem. Commun.*, 2008, **10**, 1176–1179.

26 H.-X. Zhang, A.-M. Cao, J.-S. Hu, L.-J. Wan and S.-T. Lee, Electrochemical Sensor for Detecting Ultratrace Nitroaromatic Compounds Using Mesoporous SiO$_2$-Modified Electrode, *Anal. Chem.*, 2006, **78**, 1967–1971.

27 M. Y. Ho, N. D'Souza and P. Migliorato, Electrochemical Aptamer-Based Sandwich Assays for the Detection of Explosives, *Anal. Chem.*, 2012, **84**, 4245–4247.

28 D. Zhang, J. Jiang, J. Chen, Q. Zhang, Y. Lu, Y. Yao, S. Li, G. L. Liu and Q. Liu, Smartphone-Based Portable Biosensing System Using Impedance Measurement with Printed Electrodes for 2,4,6-Trinitrotoluene (TNT) Detection, *Biosens. Bioelectron.*, 2015, **70**, 81–88.

29 T. Schüling, A. Eilers, Y. Scheper and J. Walter, Aptamer-Based Lateral Flow Assays, *AIMS Bioeng.*, 2018, **5**(2), 78–102.

30 Y. Engel, R. Elnathan, A. Pevzner, G. Davidi, E. Flaxer and F. Patolsky, Supersensitive Detection of Explosives by Silicon Nanowire Arrays, *Angew. Chem., Int. Ed.*, 2010, **49**, 6830–6835.

31 D. Gao, Z. Wang, B. Liu, L. Ni, M. Wu and Z. Zhang, Resonance Energy Transfer-Amplifying Fluorescence Quenching at the Surface of Silica Nanoparticles toward Ultrasensitive Detection of TNT, *Anal. Chem.*, 2008, **80**, 8545–8553.

32 S. Hughes, S. S. R. Dasary, S. Begum, N. Williams and H. Yu, Meisenheimer Complex between 2,4,6-Trinitrotoluene and 3-Aminopropyltriethoxysilane and Its Use for a Paper-Based Sensor, *Sens. Bio-Sens. Res.*, 2015, **5**, 37–41.

33 C. Xie, B. Liu, Z. Wang, D. Gao, G. Guan and Z. Zhang, Molecular Imprinting at Walls of Silica Nanotubes for TNT Recognition, *Anal. Chem.*, 2008, **80**(2), 437–443.

34 T. H. Lowry and K. S. Richardson, *Mechanism and Theory in Organic Chemistry*, Joanna Cotler Books, New York, NY, 3rd edn, 1987.

35 D. Gao, Z. Zhang, M. Wu, C. Xie, G. Guan and D. Wang, Surface Functional Monomer-Directing Strategy for Highly Dense Imprinting of TNT at Surface of Silica Nanoparticles, *J. Am. Chem. Soc.*, 2007, **129**, 7859–7866.

36 J. A. Wang, Simple, Rapid and Low-Cost 3-Aminopropyltriethoxysilane (APTES) Based Surface Plasmon Resonance Sensor for TNT Explosive Detection, *Anal. Sci.*, 2021, **37**, 1029–1032.

37 E. Joussein, S. Petit, J. Churchman, B. Theng, D. Righi and B. Delvaux, Halloysite Clay Minerals-a Review, *Clay Miner.*, 2005, **40**, 383–426.

38 X. Tian, W. Wang, Y. Wang, S. Komarneni and C. Yang, Polyethylenimine Functionalized Halloysite Nanotubes for Efficient Removal and Fixation of Cr (VI), *Microporous Mesoporous Mater.*, 2015, **207**, 46–52.

39 B. Szczepanik, P. Słomkiewicz, M. Garnuszek and K. Czech, Adsorption of Chloroanilines from Aqueous Solutions on the Modified Halloysite, *Appl. Clay Sci.*, 2014, **101**, 260–264.

40 P. Pal, M. K. Kundu, A. Malas and C. K. Das, Compatibilizing Effect of Halloysite Nanotubes in Polar–Nonpolar Hybrid System, *J. Appl. Polym. Sci.*, 2014, **131**, 39587.

41 H. Cai, F. Bao, J. Gao, T. Chen, S. Wang and R. Ma, Preparation and Characterization of Novel Carbon Dioxide

Adsorbents Based on Polyethylenimine-Modified Halloysite Nanotubes, *Environ. Technol.*, 2015, **36**(10), 1273–1280.

42 E. S. Goda, M. A. Gab-Allah, B. S. Singu and K. R. Yoon, Halloysite nanotubes based electrochemical sensors: A review, *Microchem. J.*, 2019, **147**, 1083–1096.

43 G. Mishra and M. Mukhopadhyay, TiO₂ Decorated Functionalized Halloysite Nanotubes (TiO₂@HNTs) and Photocatalytic PVC Membranes Synthesis, Characterization and Its Application in Water Treatment, *Sci. Rep.*, 2019, **9**(1), 4345–4361.

44 Q. Wang, J. Zhang, Y. Zheng and A. Wang, Adsorption and Release of Ofloxacin from Acid- and Heat-Treated Halloysite, *Colloids Surf., B*, 2014, **113**, 51–58.

45 P. Yuan, D. Tan and F. Annabi-Bergayal, Properties and Applications of Halloysite Nanotubes: Recent Research Advances and Future Prospects, *Appl. Clay Sci.*, 2015, **112–113**, 75–93.

46 K. Jeamjumnunja, O. Cheycharoen, N. Phongzitthiganna, S. Hannongbua and C. Prasittichai, Surface-Modified Halloysite Nanotubes as Electrochemical CO₂ Sensors, *ACS Appl. Nano Mater.*, 2021, **4**, 3686–3695.

47 B. Daglar, G. B. Demirel and M. Bayindir, Fluorescent Paper Strips for Highly Sensitive and Selective Detection of Nitroaromatic Analytes in Water Samples, *ChemistrySelect*, 2017, **2**, 7735–7740.

48 X. He, H. Wang, Z. Li, D. Chen, J. Liu and Q. Zhang, Ultrasensitive SERS Detection of Trinitrotoluene through Capillarity-Constructed Reversible Hot Spots Based on ZnO–Ag Nanorod Hybrids, *Nanoscale*, 2015, **7**, 8619–8626.

49 C. Chao, J. Liu, J. Wang, Y. Zhang, B. Zhang, Y. Zhang, X. Xiang and R. Chen, Surface Modification of Halloysite Nanotubes with Dopamine for Enzyme Immobilization, *ACS Appl. Mater. Interfaces*, 2013, **5**, 10559–10564.

50 E. Joussein, S. Petit, J. Churchman, B. Theng, D. Righi and B. Delvaux, Halloysite Clay Minerals-a Review, *Clay Miner.*, 2005, **40**, 383–426.

51 S. Jana, S. Das, C. Ghosh, A. Maity and M. Pradhan, Halloysite Nanotubes Capturing Isotope Selective Atmospheric CO₂, *Sci. Rep.*, 2015, **5**, 8711.

52 A. Ulman, Formation and Structure of Self-Assembled Monolayers, *Chem. Rev.*, 1996, **96**, 1533–1554.

53 N. Sahiner and S. B. Sengel, Environmentally Benign Halloysite Clay Nanotubes as Alternative Catalyst to Metal Nanoparticles in H₂ Production from Methanolysis of Sodium Borohydride, *Fuel Process. Technol.*, 2017, **158**, 1–8.

54 P. Yuan, P. D. Southon, Z. Liu, M. E. R. Green, J. M. Hook, S. J. Antill and C. J. Kepert, Functionalization of Halloysite Clay Nanotubes by Grafting with γ-Aminopropyltriethoxysilane, *J. Phys. Chem. C*, 2008, **112**, 15742–15751.

55 L. N. Carli, T. S. Daitx, G. V. Soares, J. S. Crespo and R. S. Mauler, The Effects of Silane Coupling Agents on the Properties of PHBV/Halloysite Nanocomposites, *Appl. Clay Sci.*, 2014, **87**, 311–319.

56 H. Li, X. Zhu, J. Xu, W. Peng, S. Zhonga and Y. Wang, Combination of Adsorption by Functionalized Halloysite Nanotubes and Encapsulation by Polyelectrolyte Coatings for Sustained Drug Delivery, *RSC Adv.*, 2016, **6**, 54463–54470.

57 D. L. Pavia, G. M. Lampman and G. S. Kriz, *Introduction to Spectroscopy: Guide for Students of Organic Chemistry*, W B Saunders, London, England, 1996.

58 A. Artemenko, A. Shchukarev, P. Štenclová, T. Wågberg, J. Segervald, X. Jia and A. Kromka, Reference XPS Spectra of Amino Acids, *IOP Conf. Ser.: Mater. Sci. Eng.*, 2021, **1050**, 012001.

59 T. C. D. Doan, J. Baggerman, R. Ramaneti, H. D. Tong, A. T. M. Marcelis and C. J. M. van Rijn, Carbon Dioxide Detection with Polyethylenimine Blended with Polyelectrolytes, *Sens. Actuators, B*, 2014, **201**, 452–459.

60 J. Xi and B. Zhang, A Non-Reductive Electrochemical Sensor for Ultrasensitive Detection of pM-Level TNT, *Anal. Methods*, 2018, **10**, 4639–4643.

61 Ş. Sağlam, A. Üzer, E. Erçağ and R. Apak, Electrochemical Determination of TNT, DNT, RDX and HMX with Gold Nanoparticles/Poly(Carbazole-Aniline) Film–Modified Glassy Carbon Sensor Electrodes Imprinted for Molecular Recognition of Nitroaromatics and Nitramines, *Anal. Chem.*, 2018, **90**, 7364–7370.

62 K. A. Mahmoud, A. Abdel-Wahab and M. Zourob, Selective Electrochemical Detection of 2,4,6-Trinitrotoluene (TNT) in Water Based on Poly(Styrene-*co*-Acrylic Acid) PSA/SiO₂/Fe₃O₄/AuNPs/Lignin-Modified Glassy Carbon Electrode, *Water Sci. Technol.*, 2015, **72**, 1780–1788.

63 M. S. Goh and M. Pumera, Graphene-Based Electrochemical Sensor for Detection of 2,4,6-Trinitrotoluene (TNT) in Seawater: The Comparison of Single-, Few-, and Multilayer Graphene Nanoribbons and Graphite Microparticles, *Anal. Bioanal. Chem.*, 2011, **399**, 127–131.

64 J. S. Stefano, A. P. Lima, C. C. Nascentes, S. R. Krzyzaniak, P. A. Mello, J. M. Gonçalves, E. M. Richter, E. Nossol and R. A. A. Munoz, Electrochemical Detection of 2,4,6-Trinitrotoluene on Carbon Nanotube Modified Electrode: Effect of Acid Functionalization, *J. Solid State Electrochem.*, 2020, **24**, 121–129.

65 H. A. Yu, J. Lee, S. W. Lewis and D. S. Silvester, Detection of 2,4,6-Trinitrotoluene Using A Miniaturized, Disposable Electrochemical Sensor with An Ionic Liquid Gel-Polymer Electrolyte Film, *Anal. Chem.*, 2017, **89**, 4729–4736.